Environmental and Climate Technologies
2020, vol. 24, no. 1, pp. 529–544
https://doi.org/10.2478/rtuect-2020-0033
https://content.sciendo.com

A Comparative Study of Dynamic Load Response of High Temperature PEM Fuel Cells

Martin TOMAS[1]*, Pavel NOVOTNY[2], Fatemeh GHOLAMI[3], Ondrej TUCEK[4], Frantisek MARSIK[5]

[1–5]*University of West Bohemia, Univerzitni 8, Pilsen, Czech Republic*

***Abstract* – The high temperature polymer electrolyte membrane fuel cell (HT-PEMFC) based on the polybenzimidazole (PBI) membrane doped with phosphoric acid (H_3PO_4) presents a promising route in the development of fuel cell technology. The higher operating temperature of 160–200 °C results in an increased tolerance of the platinum catalyst to the carbon monoxide, an improved electrode kinetics, a higher-grade heat produced by the fuel cell, and a simplified water management due to the absence of liquid water in the system. In this study, the accelerated stress test protocol (AST) corresponding to the Driving Duty Cycle was used to characterize two sets of commercial MEAs, by Danish Power Systems Ltd. and FuMA-tech GmbH, respectively. Performance characteristics prior to and after the AST procedure were measured. The changes in the resistivity of the MEA were examined by electrochemical impedance spectroscopy (EIS). The EIS data were analysed and interpreted by a suitable equivalent circuit that consisted of a resistor and the Voigt's structure in series with constant phase elements. Conducted experiments and their analysis showed suitability of the HT-PEMFC technology in applications where dynamical load of the cell is expected. Moreover, the lower number of AST cycles did not seriously affect the cell performance. As expected, with increasing number of AST cycles, decrease in the cell performance was observed. In general, presented comparative study is expected to provide an extension of existing data for present and future development of diagnostic in the field of HT-PEMFC.**

***Keywords* – Accelerated stress test; degradation; equivalent circuit; fuel cell.**

1. INTRODUCTION

The polymer electrolyte membrane fuel cells (PEMFCs) are considered as a promising alternative for stationary/portable electric power applications and ideally suited for transport applications. Well described low temperature variant (LT-PEMFC) has high power density and efficiency [1], [2], zero carbon emissions and short start-up time [3]. However, elevated operational temperature above 120 °C (HT-PEMFC), where electrolyte is based on the PBI membrane doped by phosphoric acid (PBI/H_3PO_4), is beneficial for simplified water management due to the absence of liquid water in the system and dry feed gas demands [4]–[6]. In order to improve fuel cells durability, testing protocols are designed to ensure a correct comparison of fuel cell components [7], [8]. Several testing protocols are proposed, but there is still lack of degradation studies of components currently used in high temperature fuel cells [9]–[12].

* Corresponding author.
E-mail address: mtomas@ntc.zcu.cz

There are many advantages of operating fuel cells above 120 °C, because of the enhanced electrode kinetics and a higher-grade heat produced by the fuel cell [13]. Moreover, HT-PEMFCs are more tolerant to impurities contained in reformed hydrogen [5], so the feed gas purification is easier [14]. This fact makes HT-PEMFC attractive toward the processes that produce hydrogen with higher content of carbon monoxide or carbon dioxide [15], [16]. Produced heat also allows increase of overall system efficiency in combined heat and power (CHP) units. Furthermore, flooding of the active area is avoided because the water on the cathode side is produced in its gaseous phase.

Despite these facts, many problems related to HT-PEMFC operations should be addressed. The operating temperature of the high temperature PEM fuel cells creates dry environment in the active area and this dehydration results in high ohmic losses in the electric current generation process [14]. Extreme operating conditions causes acid leaching from the HT-PEM fuel cell, which negatively affects the fuel cell performance. Higher operating temperature also leads to faster degradation of the carbon supported platinum catalyst, as reported, e.g. in [17]. Moreover, the durability and stability of the PBI based membranes, widely used in HT-PEMFC, are considered as a problem for further commercialization [18]–[20].

Wide range of operational conditions is essential for possible fuel cell applications, see [21] and references therein. Nowadays, it seems to be impractical to employ the long-term steady-state lifetime test to analyse suitability of the fuel cell technology for specific applications. Accelerated stress tests (ASTs) are used as a relevant alternative to describe the stability, reliability, and durability of a membrane electrode assembly (MEA). The load cycling accelerates degradation processes of key components; thus, the well-planned AST properly simulates the long-term testing [22]. The AST results in serious degradation processes as the membrane material loss (i.e. loss of the phosphoric acid), platinum dissolution, catalyst particles agglomeration, and corrosion of carbon materials [4], [11], [23], [24].

Furthermore, the cycling current loading conditions introduce enormous stress to the cathode side of the fuel cell, where local areas can reach a potential difference of 1.3 V causing possible carbon-support corrosion [10], [25]. The AST reduces experiment time while the crucial information about degradation processes is still provided. So, the AST plays a vital role in characterization of the fuel cells and the results are essential in the fuel cell components research and development; moreover, obtained data can be also used to set the mitigation strategies of the fuel cell degradation in the case where cycling current loading events occur [22]. However, there is still a lack of studies addressing the degradation phenomena in the field of HT-PEM fuel cells.

The present contribution focuses on the AST protocol following a new European driving duty cycle (ECE R15) and characterizing a cycle of a fuel-cell-powered car [26]. Firstly, the experimental part consisting of the test setup, and used methodology to analyse PEMFC performance and a measure of a degradation is described. Then, obtained results are discussed with respect to latter mentioned methodology. The paper is closed by a summary and a conclusion. This work is the first, to the best of the author's knowledge, to offer a complex performance study of the commercial MEA samples that have undergone ECE R15 accelerated stress test protocol.

2. METHODS AND METHODOLOGY

2.1. Test setup

The qCf FC50/125 LC V1.1 device provided by balticFuelCells connected to the Greenlight Innovation test stand G20 was utilized for MEA testing. The qCf FC50/125 LC V1.1 was extended by the cF50/125 HT CSS to measure current distribution over the MEA surface area. To heat an MEA sample, the thermostat Huber ministat 230-cc-NR with the thermofluid P20.275 50 was utilized. The first set of MEA samples was provided by Danish Power Systems, which are marketed as Dapozol®-G77 with an active area of 50 cm^2 and catalyst loading 1.3–1.5 mg Pt cm^{-2}. The second set of MEA samples was provided by FuMA-tech GmbH and these samples are distributed as Fumea® HT-PEM with an active area of 50 cm^2 and catalyst loading 1.55–1.7 mg Pt cm^{-2}. The MEA samples provided by Danish Power Systems Ltd. are labelled as D100 and D500 and the MEA samples provided by Fumatech are labelled as F100 and F500.

A test procedure, according to the new European driving duty cycle (ECE 15) [26], and JRC Scientific and Technical Reports Test Module PEFC SC 5–2 Polarisation curve for a PEFC single cell [27], was written in the Greenlight test stand scripting language. Fig. 1 shows a typical cycle of the AST procedure used to characterize the MEA samples.

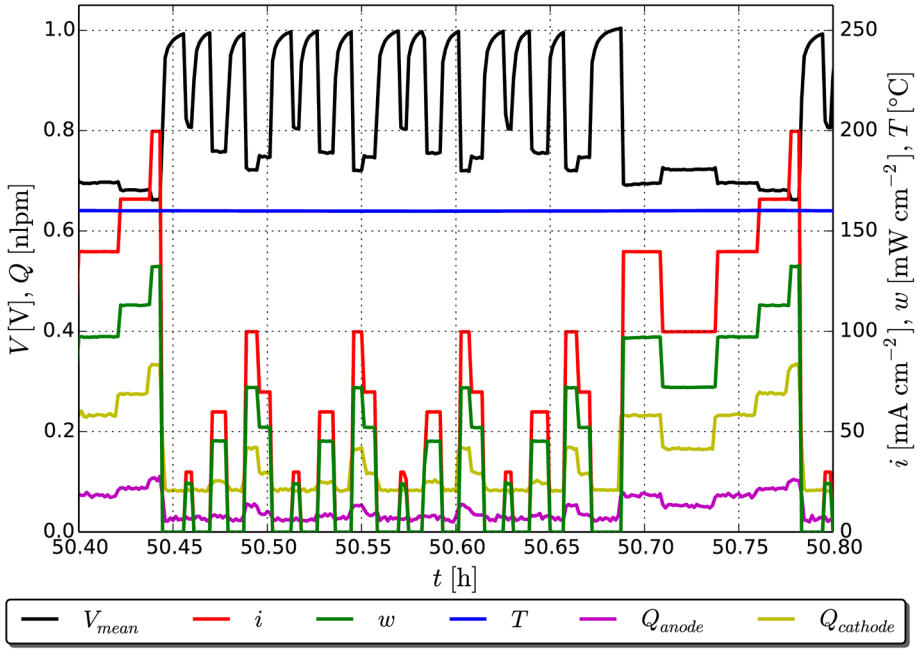

Fig. 1. Selected cycle of the test procedure. V_{mean} is the cell mean voltage, i is the cell current density, w is the cell power density, T is the cell temperature, Q_{anode} is the hydrogen volumetric flow on the anode side, $Q_{cathode}$ is the air volumetric flow on the cathode side, and t is time of the test procedure.

Focusing only on the reliability of HT-PEMFCs at the constant cell temperature of 160 °C, the inlet gases were kept at room temperature during the whole test procedure, i.e. T_{cell} = 160 °C, T_{gas} ~ 25 °C, respectively. Laboratory air with RH ~ 45–50 % (at room temperature)

was used on the cathode side and pure dry hydrogen was used on the anode side. The AST procedure were conducted for 100 and 500 cycles. So, in the case of the AST with 100 cycles, the cell worked approximately 333.3 minutes at 50 % power and 41.7 minutes at 100 % power. On the other hand, in the case of the AST with 500 cycles, the cell worked approximately 1666.7 minutes at 50 % of power and 208.3 minutes at 100 % of power. The stop condition of the AST procedure was either a total of demanded cycles or the cell voltage below 0.5 V at desired current density, whichever comes first. Similarly, the stop condition for the *i-V* curve measurement was either the cell voltage below 0.5 V or the current density above 0.4 A cm^{-2}, these stop conditions were given by limitations of the used load in the test stand. Moreover, the contact pressure on the active MEA area was kept at constant value of 1.0 N mm^{-2}.

The test procedure itself consisted of several steps as follow:

1. Heating the cell up to the temperature 160 °C;
2. Stabilising the cell for 18 hours at the temperature 160 °C in the set-up mode of the test stand, no-load connected;
3. Keeping a constant current density 0.2 A cm^{-2}, i.e. 100 % of the current demand (100 % of cell power), for 24 hours. The anode hydrogen and cathode air stoichiometry were set to 1.5 and 2.0, respectively;
4. Measuring the *i-V* curve for the constant gas stoichiometry, i.e. 1.5 for the anode and 2.0 for the cathode. Measuring the impedance spectra;
5. Performing the AST procedure consisting of 100 or 500 cycles at the anode hydrogen and cathode air stoichiometry 1.5 and 2.0, respectively. One cycle was divided into two main parts. The first part was represented by four short cycles with maximal value of the drawn current density 0.1 A cm^{-2} for 25 seconds. Duration of the one short cycle was 200 seconds. The second part was represented by one longer cycle with maximal value of the drawn current density 0.2 A cm^{-2} for 25 seconds. This second part of the cycle lasted 400 seconds. So, the whole one cycle lasted 1200 seconds;
6. Measuring the *i-V* curve for the constant gas stoichiometry, i.e. 1.5 for the anode and 2.0 for the cathode. Measuring the impedance spectra;
7. End of the test.

2.2. Electrochemical impedance spectroscopy

To understand the processes taking place in the low temperature PEMFC, impedance spectra in galvanostatic mode of the MEA samples prior to and after the AST procedure were measured by the Gamry FC-350 EIS device, which is integrated in the Greenlight Innovation G20 test stand. The impedance spectra were also measured at the constant cell temperature of 160 °C, the inlet gases were kept at room temperature during the whole test procedure, i.e. T_{cell} = 160 °C, T_{gas} ~ 25 °C, respectively. Prior to the EIS tests, conditioning of the MEA at the load of 0.2 A cm^{-2} for 15 minutes was performed. Furthermore, the anode hydrogen and cathode air stoichiometry were set to 1.5 and 2.0, respectively. Thus, the EIS tests were performed for DC 10 A, AC 0.5 A, i.e. DC 0.2 A cm^{-2} and AC 0.01 A cm^{-2}, over the frequencies ranging from 0.1 Hz to 25 kHz. Value of AC was chosen as 5 % of the DC value, which corresponds to heavy duty operating conditions [28], [29].

3. RESULTS

3.1. MEA conditioning

The cell conditioning data were obtained by drawing a current density of 0.2 A cm^{-2} for 24 hours prior to the AST procedure, this current density represents assumed working point of the fuel cell. The cell initial response is shown in Table 1 for the each MEA sample. The cell is supposed to be conditioned, if the standard deviation of the cell voltage was lower than 5 mV in the last one hour of the cell conditioning. All the MEA samples met this requirement. Each MEA was affected differently by the conditioning procedure, which is evident from mean voltage values V at the end of the conditioning procedure. Moreover, F100 and F500 show a more stable response after the conditioning procedure than D100 and D500. This is indicated by the values of voltage standard deviation V_{SD} in Table 1.

TABLE 1. INITIAL RESPONSE OF THE MEA SAMPLES, I.E THE MEAN CELL VOLTAGE V AND THE MEAN VOLTAGE STANDARD DEVIATION V_{SD} PRIOR TO THE AST PROCEDURE

Sample	V, mV	V_{SD}, mV
D100	589.3	1.1
D500	585.5	0.6
F100	670.0	0.5
F500	663.6	0.2

3.2. Dynamic cycling and degradation

The degradation caused by the AST procedure is detectable from the performance analysis. The extent of degradation is given by the differences between the performance characteristics prior to the AST procedure (beginning of test – BoT) and after the AST procedure (end of test – EoT).

The differences between the BoT and EoT characteristics of the D100 and F100 samples are not so prominent, which imply that there is no significant decrease in the performance caused by the AST procedure, see top graph in Fig. 2. On the other hand, there are considerable differences between the D100 and F100 characteristics. These differences may be connected to different MEA composition, i.e. composition of PBI/H_3PO_4 electrolyte and catalyst, MEA fabrication procedure, and also to initial properties of the MEA samples. These cogitations are supported by Table 1, where the initial MEA responses differ. So, the MEA samples by Danish Power Systems show lower initial responses, i.e. the cell voltage is lower than in the case of the MEA samples by Fumatech.

Differences between BoT and EoT characteristics are gained by higher number of the AST cycles, see bottom graph in Fig. 2. The F500 sample shows a more significant influence of the AST procedure on the performance characteristics indicating loss of performance due the dynamic load. The voltage differences of the F500 sample are 4.5 % at i = 0.1 A cm^{-2}, i.e. 50 % of cell power, and 5.4 % at i = 0.2 A cm^{-2}, i.e. 100 % of cell power. On the other hand, the voltage differences of the D500 sample are 2.4 % at i = 0.1 A cm^{-2}, i.e. 50 % of cell power, and 3.2 % at i = 0.2 A cm^{-2}, i.e. 100 % of cell power.

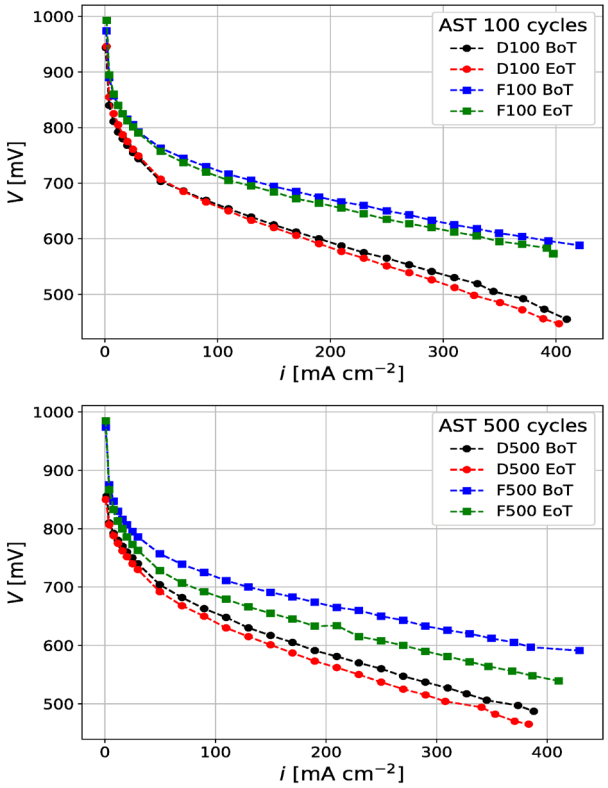

Fig. 2. Plot of the polarization curve (*i*-*V* curve) for Fumea and Dapozol MEA samples – prior to and after the AST procedure.

Furthermore, the loss of performance may be also deduced from decrease of the open circuit voltage (OCV) during the AST procedure. In the case of the MEA sample D100, the OCV decrease is 9 mV per 100 cycles. On the other hand, the MEA sample F100 shows the OCV decrease 3 mV per 100 cycles. This means that the MEA samples by Fumatech may be assumed as more stable than the MEA samples by Danish Power Systems in the case of 100 cycles. As seen from Fig. 2, an increase of the number of cycles causes the higher OCV decrease. Thus, the MEA sample F500 shows the OCV decrease 12 mV per 500 cycles, which is four times more than in the case of the 100 cycles. In the case of the MEA sample D500, the OCV decrease is 6 mV (0.7 %) per 500 cycles.

The loss of performance is also deducible from measurement of the temperature and current density distribution. It may be stated that the AST procedures with 100 cycles have no significant impact on the MEA performance, as also illustrated in Fig. 2. On the other hand, the AST procedures with 500 cycles result in more homogeneous distribution of the current density. Moreover, distribution of the temperature shows only slight variation. More details concerning these distributions are listed in the Annex.

3.3. Electrochemical impedance spectroscopy

The EIS was used as a complementary indicator of the changes in the MEA performance. The EIS measurements were performed prior to and after the AST procedure. The data representing the high-frequency resistance of the cell (HFR), see [30] and references therein, were identified from these measurements. The data confirm the elementary outcomes from the BoT and EoT performance analysis, as shown in Table 2. The HFR of the MEA sample D100 increased by 1.57 %. The similar increase was observed for the MEA sample F100. Here, the HFR increased by 2.41 %. On the contrary, the HFR of the MEA samples D500 and F500 decreased by 3.98 % and 5.15 %, respectively. These changes may be connected to the resistance to proton and electron conduction [31]. The HFR also depends on the distributed resistance of the electrolyte within the catalyst layer. The effect of drying and wetting of the membrane can be determined from the HFR [31]. Moreover, contact resistances between bipolar plates and gas diffusion layers, and gas diffusion layers and catalyst layers can also cause changes in the HFR [32]. Nevertheless, contact resistances can be neglected by constant compression of cell components as stated in [33].

TABLE 2. HIGH-FREQUENCY RESISTANCE OF THE MEA SAMPLES

Sample		HFR, mΩ
D100	BoT	3.175
	EoT	3.225
D500	BoT	1.986
	EoT	1.907
F100	BoT	2.243
	EoT	2.297
F500	BoT	1.824
	EoT	1.730

The data collected from the EIS measurement, Fig. 3, were interpreted by an equivalent circuit. As shown in Fig. 4, the equivalent circuit consisted of a resistor and the Voigt's structure in series where capacitors were replaced by constant phase elements [31]. Thus, the equivalent circuit was composed by the resistor R_{ionic} representing the resistance of the membrane, the resistor $R_{\text{CT,C}}$ representing the resistance of the charge transfer on the cathode side, the constant phase element $CPE_{\text{CT,C}}$ representing the charge transfer related capacity, the resistor $R_{\text{MT,C}}$ representing the mass transfer resistance on the cathode side and the constant phase element $CPE_{\text{MT,C}}$ representing the real mass transfer capacitance on the cathode side.

The values of the resistances R_{ionic}, $R_{\text{MT,C}}$ and $R_{\text{CT,C}}$ characterizing the equivalent circuit were determined by the Gamry Electrochem Catalysts software using the simplex method. Obtained data are summarized in Table 3. Differences between the values of the respective resistances prior to and after the AST procedure are indicated. The changes in the ionic resistance R_{ionic} follow the changes in the high-frequency resistances of the measured impedance summarized in Table 2.

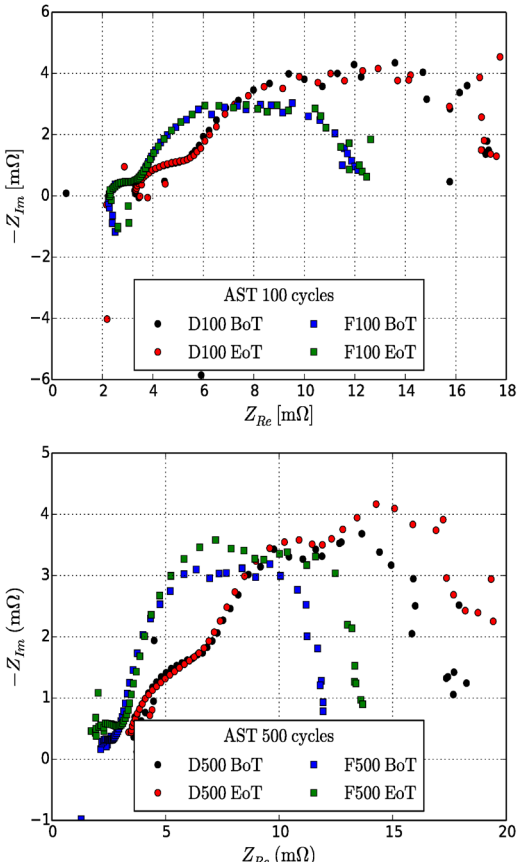

Fig. 3. Measured impedance spectra for all the MEA samples – the Nyquist plot.

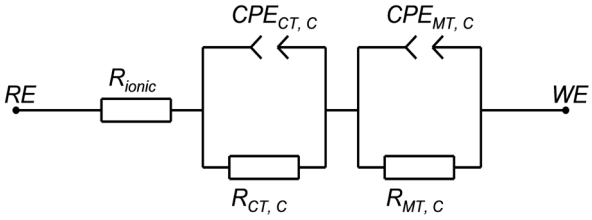

Fig. 4. Equivalent circuit of a resistor and the Voigt's structure in series with capacitors replaced by *CPE*; *RE* and *WE* represent a reference electrode and a working electrode, respectively.

TABLE 3. RESISTANCE VALUES OF THE EQUIVALENT CIRCUIT FOR THE INDIVIDUAL MEA

Sample		R_{ionic}, mΩ	$R_{MT,C}$, mΩ	$R_{CT,C}$, mΩ
D100	BoT	3.222	1.747	13.010
	EoT	3.278	1.605	14.060
D500	BoT	2.002	0.168	15.040
	EoT	1.905	0.262	15.390
F100	BoT	2.312	0.853	9.380
	EoT	2.342	0.814	9.634
F500	BoT	1.842	0.942	9.793
	EoT	1.770	1.191	11.130

The change in R_{ionic} may present a measure of the variations in membrane properties due to the AST procedure, because the cyclic stress tests generate through-thickness cracks, in-plane tears, and local thinning of the polymer membrane, which diminish ionic conductivity [34]. So that, the R_{ionic} of the MEA samples D100 and F100 increased by 1.74 % and 1.30 %, respectively; whereas R_{ionic} of the MEA samples D500 and F500 decreased by 4.85 % and 3.91 %, respectively. Resistances associated with transfer of reactant gasses to electrode active sites are represented by $R_{MT,C}$. Thus, $R_{MT,C}$ varies when new pathways for the reactant flow to the catalyst layer are created or when some existing pathways are blocked [35]. However, the increase of $R_{MT,C}$ can be attributed to decrease in CCL (cathode catalyst layer) thickness, as reported in [36]. The investigated MEA samples show both type of described behaviour. So, $R_{MT,C}$ values in the case of the MEA samples D100 and F100 decreased by 8.13 % and 4.57 %, respectively, indicating opening of the new pathways for reactant flow due to the AST procedure. On contrary, $R_{MT,C}$ values in the case of the MEA samples D500 and F500 increased by 55.95 % and 26.43 %, respectively, meaning the thinning of the CCL due to the AST procedure. The level of hydration of the electrolyte contained in the electrode (CCL) relates to the changes in $R_{CT,C}$ [35]. To be more specific, the resistor $R_{CT,C}$ describes the cathode double layer, which is a barrier between the surface of the electrode and the absorbed species. The resistances $R_{CT,C}$ of the all MEA samples increased. This increase was in the case of the MEA samples D100 and F100 8.07 % and 2.71 %, respectively; and in the case of the MEA samples D500 and F500 it was 2.33 % and 13.65 %, respectively. Moreover, these changes may be correlated with the catalyst layer decomposition and with the formation of more complex double layer due to the AST procedure.

Results for the MEA sample D100 with F100 and the MEA sample D500 with F500 show that the MEA samples by Fumatech, i.e. F100 and F500, are relatively more stable to a dynamic load cycle presented by the AST procedure.

4. CONCLUSION

This report presents a characterization of MEA samples for the high temperature PEMFC working at the constant temperature 160 °C and under a dynamic load in terms of an AST procedure consisting of 100 and 500 cycles. The performance characteristics and impedance spectra prior to and after the AST procedure were compared.

The performance analysis was made for four investigated MEA samples provided by Danish Power Systems Ltd., samples D100 and D500, and by FuMA-tech GmbH, samples F100 and F500, respectively. The main outcomes of carried out analysis may be summarized as follows:

the initial responses of the F100 and F500 samples are more stable than of the D100 and D500 samples (to be more specific, the standard deviations of D100 and D500 samples were 1.1 mV and 0.6 mV, respectively, but the standard deviations of F100 and F500 samples were 0.5 and 0.2, respectively); the real impedance of the MEA samples tested for 100 cycles, i.e. D100 and F100, increased during the AST procedure, whereas the real impedance of the MEA samples tested for 500 cycles, i.e. D500 and F500, decreased during the AST procedure. So, an increase and a decrease in the high-frequency resistances are observed as illustrated by the EIS analysis. According to the carried-out analysis, it may be stated that the MEA samples by FuMA-tech, i.e. F100 and F500, showed relatively more stable responses to the AST procedure than the MEA samples provided by Danish Power Systems, i.e. D100 and D500. This is demonstrated by the high-performance behaviour of the MEA samples depicted in Fig. 2. The maximal EoT current density of D100 and D500 samples was 402.62 A cm^{-2} at 447 mV and 383.29 A cm^{-2} at 465 mV, respectively, whereas the maximal EoT current density of F100 and F500 samples was 397.58 A cm^{-2} at 573 mV and 410.52 A cm^{-2} at 539 mV, respectively.

Thus, the accelerated stress test procedures are confirmed to be a useful technique to characterize the hydrogen PEMFC performance under non-steady conditions. Moreover, they enable to investigate various operations under realistic conditions in a shorter time, which can support usage of this technology in real applications. The future research should evaluate the MEA samples from other providers (or modified MEA samples) and extend the AST protocol to higher number of cycles. Other methods of MEA samples characterization should be employed for deeper understanding of MEA degradation. Then, the results could be used to design the optimization and mitigation strategies. The different properties of the MEA samples (even from the same provider) should be minimized by conducting the same procedure with more than one MEA in order to increase the reproducibility of the measurement.

ACKNOWLEDGEMENT

The result was developed within the CENTEM project, reg. no. CZ.1.05/2.1.00/03.0088, co-funded by the ERDF as part of the Ministry of Education, Youth and Sports OP RDI programme and, in the follow-up sustainability stage, supported through CENTEM PLUS (LO1402) by financial means from the Ministry of Education, Youth and Sports under the National Sustainability Programme I.

REFERENCES

[1] Staffell I., Scamman D., Abad A. V., Balcombe P., Dodds P. E., Ekins P., Shah N., Ward K. R. The role of hydrogen and fuel cells in the global energy system. *Energy & Environmental Science* 2019:12:463–491. https://doi.org/10.1039/C8EE01157E

[2] Blumberga D., Chen B., Ozarska A., Indzere Z., Lauka D. Energy, Bioeconomy, Climate Changes and Environment Nexus. *Environmental and Climate Technologies* 2019:23:370–392. https://doi.org/10.2478/rtuect-2019-0102

[3] Wang Y., Chen K. S., Mishler J., Cho S. C., Adroher X. C. A review of polymer electrolyte membrane fuel cells: Technology, applications, and needs on fundamental research. *Applied Energy* 2011:88(4):981–1007. https://doi.org/10.1016/j.apenergy.2010.09.030

[4] Zhang J., Xie Z., Zhang J., Tang Y., Song C., Navessin T., Shi Z., Song D., Wang H., Wilkinson D. P., Liu Z.-S., Holdcroft S. High temperature PEM fuel cells. *Journal of Power Sources* 2006:160(2):872–891. https://doi.org/10.1016/j.jpowsour.2006.05.034

[5] Yang C., Costamagna P., Srinivasan S., Benziger J., Bocarsly A. B. Approaches and technical challenges to high temperature operation of proton exchange membrane fuel cells. *Journal of Power Sources* 2001:103(1):1–9. https://doi.org/10.1016/S0378-7753(01)00812-6

[6] Pan C., He R., Li Q., Jensen J. O., Bjerrum N. J., Hjulmand H. A., Jensen A. B. Integration of high temperature PEM fuel cells with a methanol reformer. *Journal of Power Sources* 2005:145(2):392–398. https://doi.org/10.1016/j.jpowsour.2005.02.056

[7] Büsselmann J., Rastedt M., Tullius V., Yezerska K., Dyck A., Wagner P. Evaluation of HT-PEM MEAs: Load cycling versus start/stop cycling. *International Journal of Hydrogen Energy* 2019:44(35):19384–19394. https://doi.org/10.1016/j.ijhydene.2018.07.181

[8] Büsselmann J., Rastedt M., Klicpera T., Reinwald K., Schmies H., Dyck A., Wagner P. Analysis of HT-PEM MEAs' Long-Term Stabilities. *Energies* 2020:13(3):567. https://doi.org/10.3390/en13030567

[9] Jeon Y., Na H., Hwang H., Park J., Hwang H., Shul Y.-G. Accelerated life-time test protocols for polymer electrolyte membrane fuel cells operated at high temperature. *International Journal of Hydrogen Energy* 2015:40(7):3057–3067. https://doi.org/10.1016/j.ijhydene.2015.01.010

[10] Kannan A., Kabza A., Scholta J. Long-term testing of start-stop cycles on high temperature PEM fuel cell stack. *Journal of Power Sources* 2015:277:312–316. https://doi.org/10.1016/j.jpowsour.2014.11.115

[11] Zhang S., Yuan X., Wang H., Merida W., Zhu H., Shen J., Wu S., Zhang J. A review of accelerated stress tests of MEA durability in PEM fuel cells. *International Journal of Hydrogen Energy* 2009:34:388–404. https://doi.org/10.1016/j.ijhydene.2008.10.012

[12] Schonvogel D., Rastedt M., Wagner P., Wark M., Dyck A. Impact of Accelerated Stress Tests on High Temperature PEMFC Degradation. *Fuel Cells* 2016:16(4):480–489. https://doi.org/10.1002/fuce.201500160

[13] Rosli R. E., Sulong A. B., Daud W. R. W., Zulkifley M. A., Husaini T., Rosli M. I., Majlan E. H., Haque M. A. A review of high – temperature proton exchange membrane fuel cell (HT-PEMFC) system. *International Journal of Hydrogen Energy* 2017:42(14):9293–9314. https://doi.org/10.1016/j.ijhydene.2016.06.211

[14] Chandan A., Hattenberger M., El-kharouf A., Du S., Dhir A., Self V., Pollet B. G., Ingram A., Bujalski W. High temperature (HT) polymer electrolyte membrane fuel cells (PEMFC) – A review. *Journal of Power Sources* 2013:231:264–278. https://doi.org/10.1016/j.jpowsour.2012.11.126

[15] Klavins M., Bisters V., Burlakovs J. Small Scale Gasification Application and Perspectives in Circular Economy. *Environmental and Climate Technologies* 2018:22:42–54. https://doi.org/10.2478/rtuect-2018-0003

[16] Ozola Z. U., Vesere R., Kalnins S. N., Blumberga D. Paper Waste Recycling. Circular Economy Aspects. *Environmental and Climate Technologies* 2019:23:260–273. https://doi.org/10.2478/rtuect-2019-0094

[17] Stevens D. A., Dahn J. R. Thermal degradation of the support in carbon-supported electrocatalysts for PEM fuel cells. *Carbon* 2005:43(1):179–188. https://doi.org/10.1016/j.carbon.2004.09.004

[18] Daud N. A. B, Abouzari Lotf E., Sophia Sha'rani S., Nasef M. M., Ahmad A., Rasit Ali R. Efforts to Improve PBI/Acid Membrane System for High Temperature Polymer Electrolyte Membrane Fuel Cell (HT-PEMFC). *E3S Web of Conferences* 2019:90:01002. https://doi.org/10.1051/e3sconf/20199001002

[19] Zhang J., Aili D., Lu S., Li Q., Jiang S. P. Advancement toward Polymer Electrolyte Membrane Fuel Cells at Elevated Temperatures. *AAAS Research* 2020:2020:9089405. https://doi.org/10.34133/2020/9089405

[20] Sun X., Simonsen S. C., Norby T., Chatzitakis A. Composite Membranes for High Temperature PEM Fuel Cells and Electrolysers: A Critical Review. *Membranes* 2019:9(7):83. https://doi.org/10.3390/membranes9070083

[21] Sharaf O. Z., Orhan M. F. An overview of fuel cell technology: Fundamentals and applications. *Renewable & Sustainable Energy Reviews* 2014:32:810–853. https://doi.org/10.1016/j.rser.2014.01.012

[22] Wu J., Yuan X. Z., Martin J. J., Wang H., Zhang J., Shen J., Wu S., Merida W. A review of PEM fuel cell durability: Degradation mechanisms and mitigation strategies. *Journal of Power Sources* 2008:184(1):104–119. https://doi.org/10.1016/j.jpowsour.2008.06.006

[23] Park J. O., Hong S.-G. Design and optimization of HT-PEMFC MEAs. In: Li Q., Aili D., Hjuler H.A., Jensen J.O. (eds.), *High temperature polymer electrolyte membrane fuel cells*. Dordrecht: Springer, 2016, 331–352. https://doi.org/10.1007/978-3-319-17082-4_16

[24] Lai Y.-H., Rahmoeller K. M., Hurst J. H., Kukreja R. S., Atwan M., Maslyn A. J., Gittleman C. S. Accelerated Stress Testing of Fuel Cell Membranes Subjected to Combined Mechanical/Chemical Stressors and Cerium Migration, *Journal of the Electrochemical Society* 2018:165:F3217–F3229. https://doi.org/10.1149/2.0241806jes

[25] Spernjak D., Fairweather J., Rockward T., Mukundan R., Borup R. L. Characterization of carbon corrosion in a segmented PEM fuel cell. *ECS Transactions* 2011:41:741–750. https://doi.org/10.1149/1.3635608

[26] Bloom I., Walker L. K., Basco J. K., Malkow T., Saturnio A., De Marco G., Tsotridis G. A comparison of fuel cell testing protocols – A case study: Protocols used by the U.S. Department of Energy, European Union, International Electrotechnical Commission/Fuel Cell Testing and Standardization Network, and Fuel Cell Technical Team. Journal of Power Sources 2013:243:451–457. https://doi.org/10.1016/j.jpowsour.2013.06.026

[27] FCTestNet/FCTes^{QA}. Test module PEFC SC 5-2. Testing the voltage and the power as a function of the current density. Polarisation curve for a PEFC single cell. Technical report, European Commission Joint Research Centre, Institute for Energy, 2010.

[28] Gode P., Jaouen F., Lindbergh G., Lundblad A., Sundholm G. Influence of the composition on the structure and electrochemical characteristics of the PEFC cathode. *Electrochimica Acta* 2003:48(28):4175–4187. https://doi.org/10.1016/S0013-4686(03)00603-0

[29] Yuan X. Z., Wang H., Sun J. C., Zhang J. AC impedance technique in PEM fuel cell diagnosis – A review. *International Journal of Hydrogen Energy* 2007:32(17):4365–4380. https://doi.org/10.1016/j.ijhydene.2007.05.036
[30] Cooper K. R., Smith M. Electrical test methods for on-line fuel cell ohmic resistance measurement. *Journal of Power Sources* 2006:160(2):1088–1095. https://doi.org/10.1016/j.jpowsour.2006.02.086
[31] Yuan X. Z., Song C., Wang H., Zhang J. *Electrochemical impedance spectroscopy in PEM fuel cells: Theory and practice*. London: Springer, 2010. https://doi.org/10.1007/978-1-84882-846-9
[32] Jespersen J. L., Schaltz E., Kaer S. K. Electrochemical characterization of a polybenzimidazole-based high temperature proton exchange membrane unit cell. *Journal of Power Sources* 2009:191(2):289–296. https://doi.org/10.1016/j.jpowsour.2009.02.025
[33] Chang W. R., Hwang J. J., Weng F. B., Chan S. H. Effect of clamping pressure on the performance of a PEM fuel cell. *Journal of Power Sources* 2007:166(1):149–154. https://doi.org/10.1016/j.jpowsour.2007.01.015
[34] Mukundan R., Baker A. M., Kusoglu A., Beattie P., Knights S., Weber A. Z., Borup R. L. Membrane Accelerated Stress Test Development for Polymer Electrolyte Fuel Cell Durability Validated Using Field and Drive Cycle Testing. *Journal of the Electrochemical Society* 2018:165:F3085–F3093. https://doi.org/10.1149/2.0101806jes
[35] Yuan X. Z., Sun J. C., Wang H., Li H. Accelerated conditioning for a proton exchange membrane fuel cell. *Journal of Power Sources* 2012:205:340–344. https://doi.org/10.1016/j.jpowsour.2012.01.039
[36] Stariha S., Macauley N., Sneed B. T., Langlois D., More K. L., Mukundan R., Borup R. L. Recent Advances in Catalyst Accelerated Stress Tests for Polymer Electrolyte Membrane Fuel Cells. *Journal of the Electrochemical Society* 2018:165:F492–F501. https://doi.org/10.1149/2.0881807jes

Martin Tomas, Ph.D., researcher in New Technologies, Research Centre, University of West Bohemia. He defended Ph.D. thesis in 2011 in University of West Bohemia (Czech Republic). The main research areas are hydrogen PEM fuel cells, material characterization and theoretical approaches based on non-equilibrium thermodynamics.
E-mail: mtomas@ntc.zcu.cz
ORCID iD: https://orcid.org/0000-0001-7834-280X

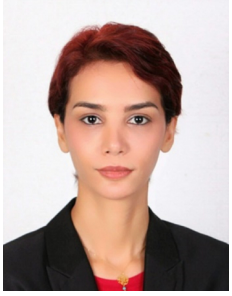

Fatemeh Gholami, Ph.D., received her BSc and MSc in chemical engineering 2002 and 2009, respectively. She obtained PhD in Chemical Engineering (Nanoscience and Technology) at the Universiti Sains Malaysia in 2014. She continued research at University of Malaya and Universiti Sains Malaysia. Currently, she is researcher in the New Technologies-Reseach Centre/ West Bohemia University (UWB) in Pilsen, Czech Republic. Her research interests are biomaterials, nanotechnology, air pollution removal, water treatment and wastewater engineering, and surface analysis of materials.
E-mail: gholami@ntc.zcu.cz
ORCID iD: http://orcid.org/0000-0003-2665-5155

Pavel Novotny received the M.Sc. degree in mechanical engineering at the Czech Technical University in Prague in 2007. The main research areas cover modeling of electrochemical processes in PEM fuel cells (FEM), accelerated stress tests of PEM fuel cells, and sorption analysis of materials.
E-mail: novot.pav@gmail.com

Ondřej Tuček, M.Sc., researcher in New Technologies - Research Centre, University of West Bohemia. He obtained a master of degree in 2008 at the University of West Bohemia (Czech Republic), where he was studying an applied mathematics at Faculty of Applied Sciences. The main research areas cover programming of optimization and control process for fuel cells.
E-mail: otucek@ntc.zcu.cz
ORCID iD: http://orcid/0000-0003-2495-0396

František Maršík, Prof., Dr. Sc., born 1942, PhD received in Thermodynamics and fluid mechanics at the Institute of thermomechanics, Czech Academy of Sciences in 1974. From 1999 he is Professor of Fluid mechanics and thermodynamics at Czech Technical University and Charles University in Prague. In 2011 he joined New Technologies - Research Centre, University of West Bohemia, Czech Republic. The main research interest is the irreversible thermodynamics and its applications to the problems of the phase transition kinetics, thermo-hydrodynamic stability of fluids and hydrogen fuel cells.
E-mail: marsik@it.cas.cz

ANNEX

For measurement of distribution of the current density was utilized the cF50/125 HT CSS, which extended the qCf FC50/125 LC V1.1 provided by balticFuelCells. This device partitions a MEA surface into individual segments in ratio 10×14 in axes *x, y* and enables simultaneous measurement of the temperature and current density of a segment, see Fig. A1. The temperature and current density values were acquired in each cycle during a period of the maximal load lasting 25 seconds, i.e. at the current density 0.2 A cm^{-2}.

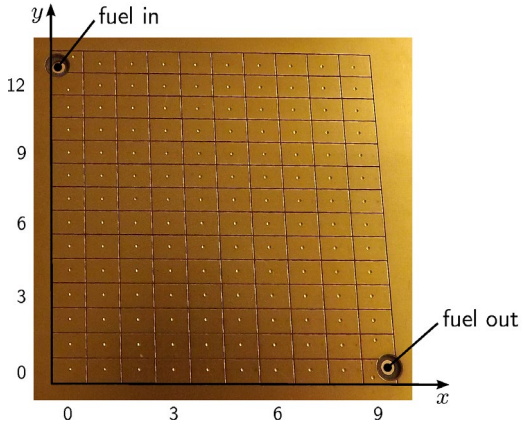

Fig. A1. Scheme of current scan segments.

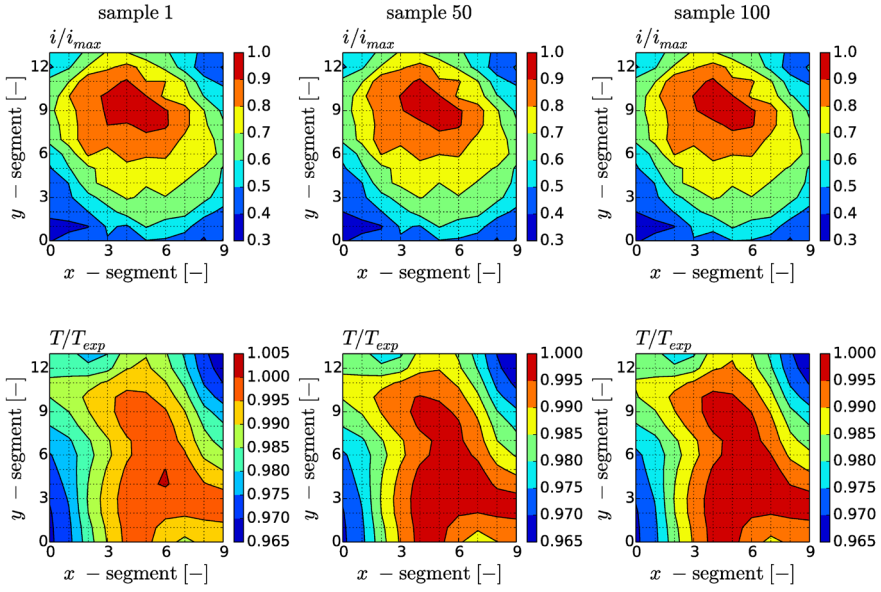

Fig. A2. Distribution of the current density and temperature at maximal load in the AST - D100.

The MEA samples D100 and F100 show no significant variation in distribution of the temperature and current density due to AST procedure, see Figs. A2 and Fig. A3. Distribution of the temperature reflects inlet (segment approx. 8×2) and outlet (segment approx. 1×12) of the thermofluid into the cell meaning that the temperature decreases towards outlet. Distribution of the current density also reflects inlet and outlet of the fuel, depicted in Fig. A2. It means that areas with the higher current density can be found in the upper half of the MEA samples. Moreover, the sample F100 shows more homogeneous distribution of the current density compared to the sample D100.

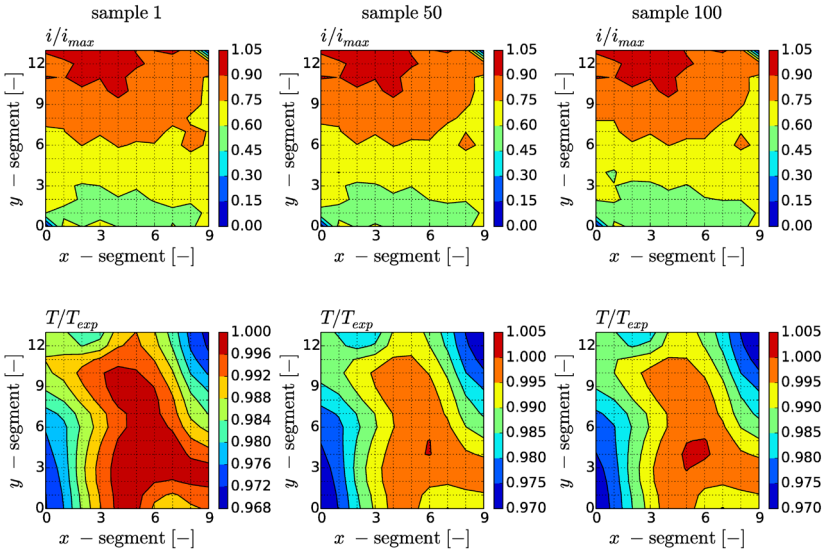

Fig. A3. Distribution of the current density and temperature at maximal load in the AST - F100.

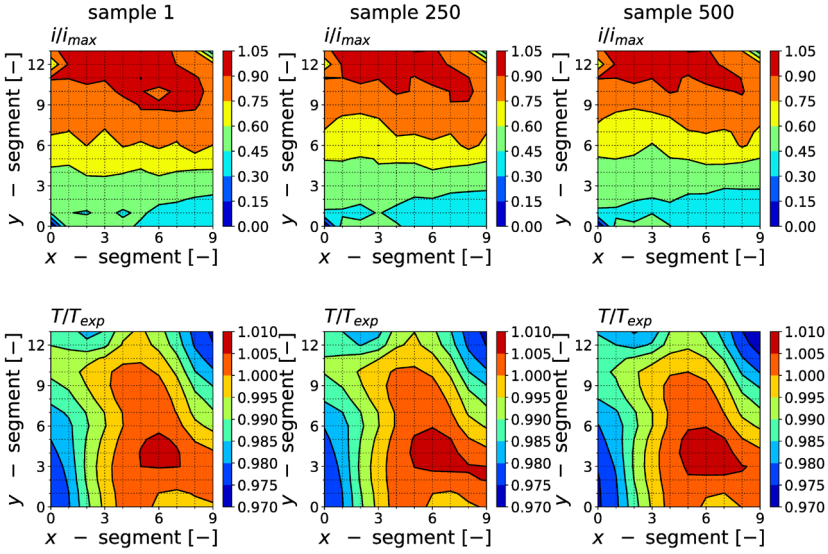

Fig. A4. Distribution of the current density and temperature at maximal load in the AST - D500.

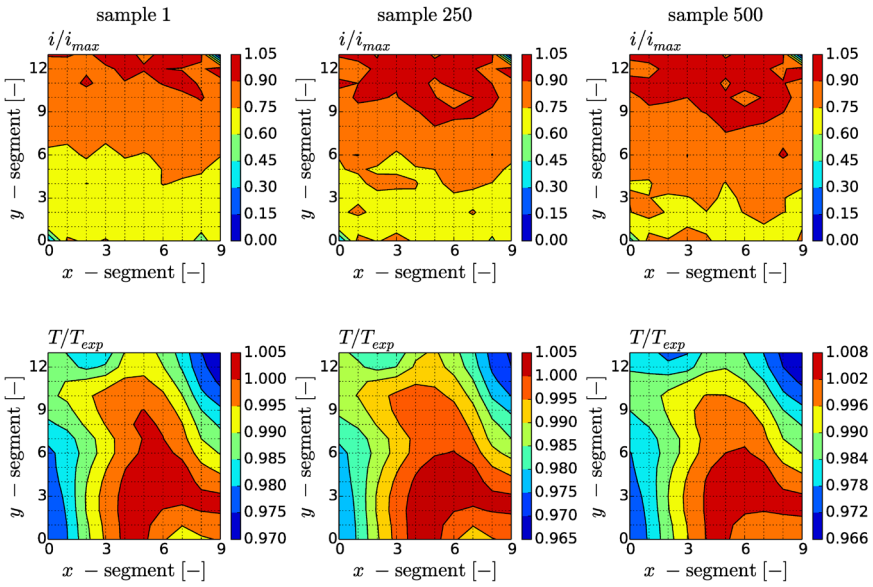

Fig. A5. Distribution of the current density and temperature at maximal load in the AST - F500.

The MEA samples D500 and F500 show impact of the AST procedure on distribution of the temperature and current density, see Figs. A4 and Fig. A5. As in the previous cases, distribution of the temperature reflects inlet (segment approx. 8×2) and outlet (segment approx. 1×12) of the thermofluid into the cell meaning that the temperature decreases towards outlet. Due to the AST procedure, slight changes in distribution of the temperature may be identified. Distribution of the current density corresponds to inlet and outlet of the fuel, as indicated in Fig. 5. Furthermore, distribution of the current density varies with increasing number of cycles meaning that area with the lower current density relatively decreases as the AST cycles approaches value 500. It can be also stated that the sample F500 shows more homogeneous distribution of the current density compared to the sample D500 as in the case of the 100 cycles.